RESEARCH ARTICLE

Atomically dispersed Mn for electrochemical CO_2 reduction with tunable performance

Zhibo Yao[a], Xinyu Zhan[a], Yukun Ruan[a], Weixiang Li[a], Yiwen Xu[a], Yuxin Chen[a], Alex W. Robertson[b], Song Hong*[a], Leiduan Hao*[a] and Zhenyu Sun*[a]

[a] Z. Yao, X. Zhan, Y. Ruan, W. Li, Y. Xu, Prof. S. Hong, Prof. L. Hao, Prof. Z. Sun
State Key Laboratory of Chemical Resource Engineering, College of Chemical Engineering
Beijing University of Chemical Technology
Beijing, 100029, P. R. China
E-mail: haold@buct.edu.cn, sunzy@mail.buct.edu.cn
[b] Dr. A. W. Robertson
Department of Physics
University of Warwick
Coventry, CV4 7AL, U. K.

Supporting information for this article is given via a link at the end of the document.

Abstract: Electrochemical CO_2 reduction (ECR) is recognized as a sustainable and promising means to producing valuable chemicals. To facilitate widespread application of this technology, the design and construction of efficient cathodic electrocatalysts is critically important. Here we report facile and scalable synthesis of atomically dispersed manganese (Mn) on nitrogen-doped porous carbon (NC) for active ECR reaction to CO. The as-obtained Mn single atoms (Mn SAs) deliver high activity and selectivity toward CO formation with a faradaic efficiency of 80.5 ± 0.6 % at −0.8 V (versus reversible hydrogen electrode) in 0.1 M $KHCO_3$ solution using an H-type cell, over 5 times that of bare NC. The high activity is preserved even after 10 h of continuous polarization. The catalytic properties of the cost-effective Mn SAs/NC are readily tuned by regulating N configurations and the percentage of Mn SAs via modulation of N precursor and thermal treatment conditions.

Introduction

Electrochemical CO_2 reduction (ECR) to value-added compounds can be driven by electricity from green and renewable sources using hydrogen generated in situ from water electrolysis instead of blue H_2 from fossil fuels, thus providing a potential route to ameliorate the greenhouse effect and close the carbon cycle. [1–6] Among the various products of ECR, CO is one of the most practical target compounds which is a critical feedstock for multiple important reactions, such as the water-gas shift reaction, Fischer-Tropsch process, and methanol synthesis, among others. Converting CO_2 to CO via electrolysis is posited to proceed through three steps by transferring two electrons. [7–10] A CO_2 molecule is first transformed to a *COOH intermediate (* represents an adsorbed site) via either a concerted proton/electron transfer or formation of a $CO_2^{\bullet-}$ anion, which is subsequently converted to *CO after attacking of the oxygen atom in the *COOH by the 2nd proton/electron pair, followed by desorption of *CO from the catalyst surface. Noble metals such as Au and Ag have been demonstrated to be able to catalyze the ECR to CO. [11–13] Whereas their high costs and limited reserves restrain large-scale applications of the precious metals. It is known that the generation of CO is often accompanied by the concurrent evolution of H_2 resulting from the competing proton or water reduction reaction. Therefore, developing an earth-abundant and cost-effective electrocatalyst that can thwart the parasitic hydrogen evolution reaction (HER) while boost the ECR is highly desired.

Recently, single-atom catalysts (SACs) with a concept of "isolated active site within a solid catalyst" have attracted increasing attention since the pioneering work by Zhang et al. in 2011 The performance of supported catalysts tends to increase with decreasing metal particle size and size distributions. [14] SACs maximize atom utilization efficiency. Meanwhile, the quantum size effect, unsaturated coordination state, and peculiar interaction between metal atoms and support lead to extremely high activity and selectivity. [15–22] In addition, SACs characterized with homogenous catalytic active centers offer a simple model for mechanistic investigations. From this context, a range of emerging SACs including sp post-transition metals and late transition metals have been employed in the field of ECR. [23–27] However, single-atom electrocatalysis on manganese (Mn), the third most abundant transition metal in the crust, has been rarely studied in the ECR. Zhang et al. fabricated a family of SACs with a variety of transition metals, including Mn SACs which exhibited a low CO faradaic efficiency (FE) of only about 61%. [28] Likewise, a similar FE toward CO formation (65%) was attained on a Mn-N-C catalyst by Strasser and co-workers. [29] Thus, it is desired to further tune and optimize the interaction of Mn and N-doped carbon support and its electronic structure on the surface to afford high-efficiency ECR toward CO.

Here, we report a facile and scalable method for the synthesis of atomically dispersed Mn on the surface of N-doped porous carbon (Mn SAC/NC) via annealing of the complex of 2,2'-bipyridine-5,5'-dicarboxylic acid and Manganese acetate tetrahydrate immobilized on carbon black. The as-prepared Mn SAC/NC displays remarkable activities for the ECR to produce CO, with a maximum FE exceeding 80%, outperforming the previously reported Mn-N-C catalysts. Especially, the ECR properties are readily tuned by manipulation of N-containing precursor type, loading of Mn, and thermal treatment temperature. The electrocatalyst can sustain at least 10 h of continuous CO_2 electrolysis without appreciable loss of catalytic activity.

Results and Discussion

Morphological and structural investigation

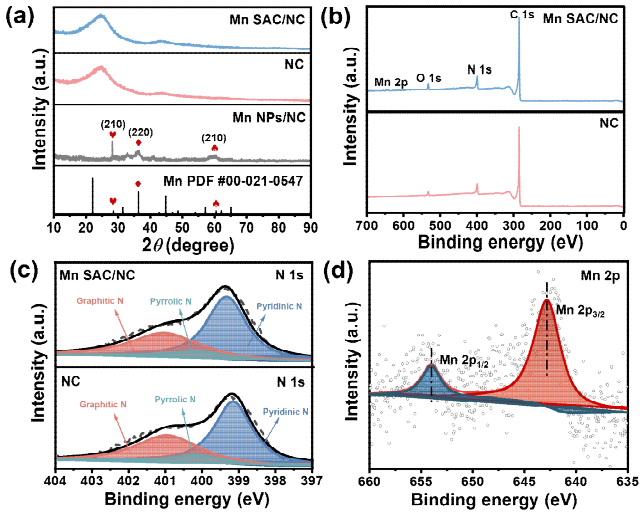

Figure 1. (a) XRD patterns of Mn SAC/NC, NC, and Mn NPs/NC. (b) Wide-survey XPS spectra and (c) N 1s XPS spectra of Mn SAC/NC and NC. (d) Mn 2p XPS spectrum of Mn SAC/NC.

The Mn SAC/NC was prepared via a simple impregnation and calcination method using manganese acetate tetrahydrate and 2,2'-bipyridine-5,5'-dicarboxylic acid as the respective metal precursor and nitrogen source and activated carbon as catalyst support. By controlling Mn loading, atomically dispersed Mn sites were decorated on the surface of N-doped carbon (NC), namely Mn SAC/NC. For comparison, neat NC and Mn nanoparticles on NC (Mn NPs/NC) were also prepared. X-ray diffraction (XRD) measurements were first performed to investigate the crystalline structure of the as-obtained samples. As shown in Figure 1a, both Mn SAC/NC and NC display two broad peaks at ~24 and 47° that are typical for carbon materials with low crystallinity. No diffraction peaks assigned to Mn species were detected for Mn SAC/NC, excluding the presence of large crystalline Mn-related particles. For Mn NPs/NC, pronounced diffraction peaks are observable, which can be attributed to metallic Mn (PDF 021-0547), indicating the formation of Mn NPs supported on NC. The surface composition and oxidation state of the samples were explored using X-ray photoelectron spectroscopy (XPS). The full-scan XPS spectra (Figure 1b) confirmed the existence of Mn, O, N, and C in Mn SAC/NC without other impurities. In both NC and Mn SAC/NC, the N 1s spectra (Figure 1c) can be deconvoluted into three peaks centered at ~399.3, ~400, and ~401 eV corresponding to graphitic N, pyrrolic N, and pyridinic N, respectively. For Mn SAC/NC, the Mn 2p spectrum showed a spin-orbit split doublet with Mn $2p_{1/2}$ at ~654.1 eV and $2p_{3/2}$ at ~642.9 eV, which was assigned to Mn^{2+}. [30]

The morphology and structure of Mn SAC/NC were further examined by transmission electron microscopy (TEM) and scanning transmission electron microscopy (STEM). Plenty of spheres with diameters of about 30 nm can be seen (Figure 2a–b). A semi-graphite "onion shell" morphology of the NC support is clearly observed. No metal clusters or nanoparticles were found, consistent with the XRD results. Further aberration corrected high-angle annular dark-field STEM provided direct proof of the presence of Mn atoms Owing to the higher atomic number of Mn than that of C and N, the bright dots shown in Figure 2c–d) can be attributed to Mn single atoms. The energy-dispersive X-ray spectroscopy (EDS) elemental maps of Mn SAC/NC (Figure 2e) illustrated the uniform distribution of Mn, N, and C on the entire NC support. The above characterization results verified the formation of atomically dispersed Mn species on the surface of NC matrix.

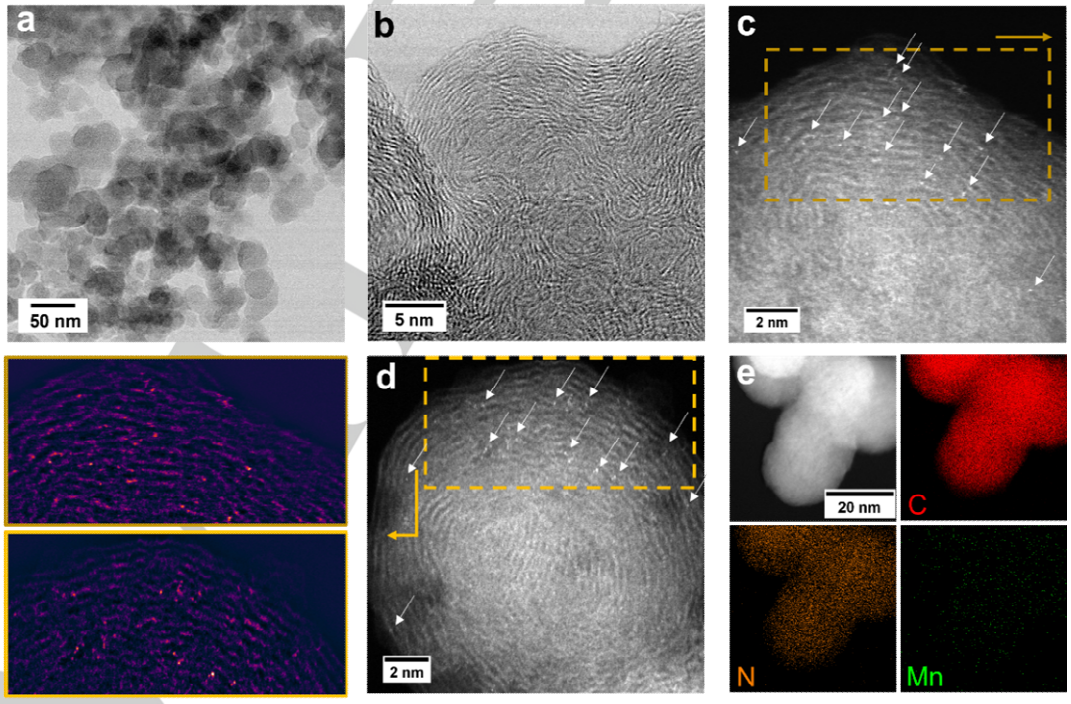

Figure 2. (a) TEM image for Mn SAC/NC. (b) Bright field (BF) STEM image of the carbon support, showing the semi-graphitic 'onion shell' structure. (c) and (d) High magnification HAADF STEM images of bright Mn single atoms decorating the carbon shells, indicated by white arrows. Indicated boxed areas are shown as accompanying false-color lookup table images following bandpass filtering, showing the bright Mn atoms. (e) EDX maps for Mn SAC/NC.

Electrochemical performance analysis

current densities than NC, suggesting that Mn SAC/NC possessed higher ECR catalytic activity than NC.

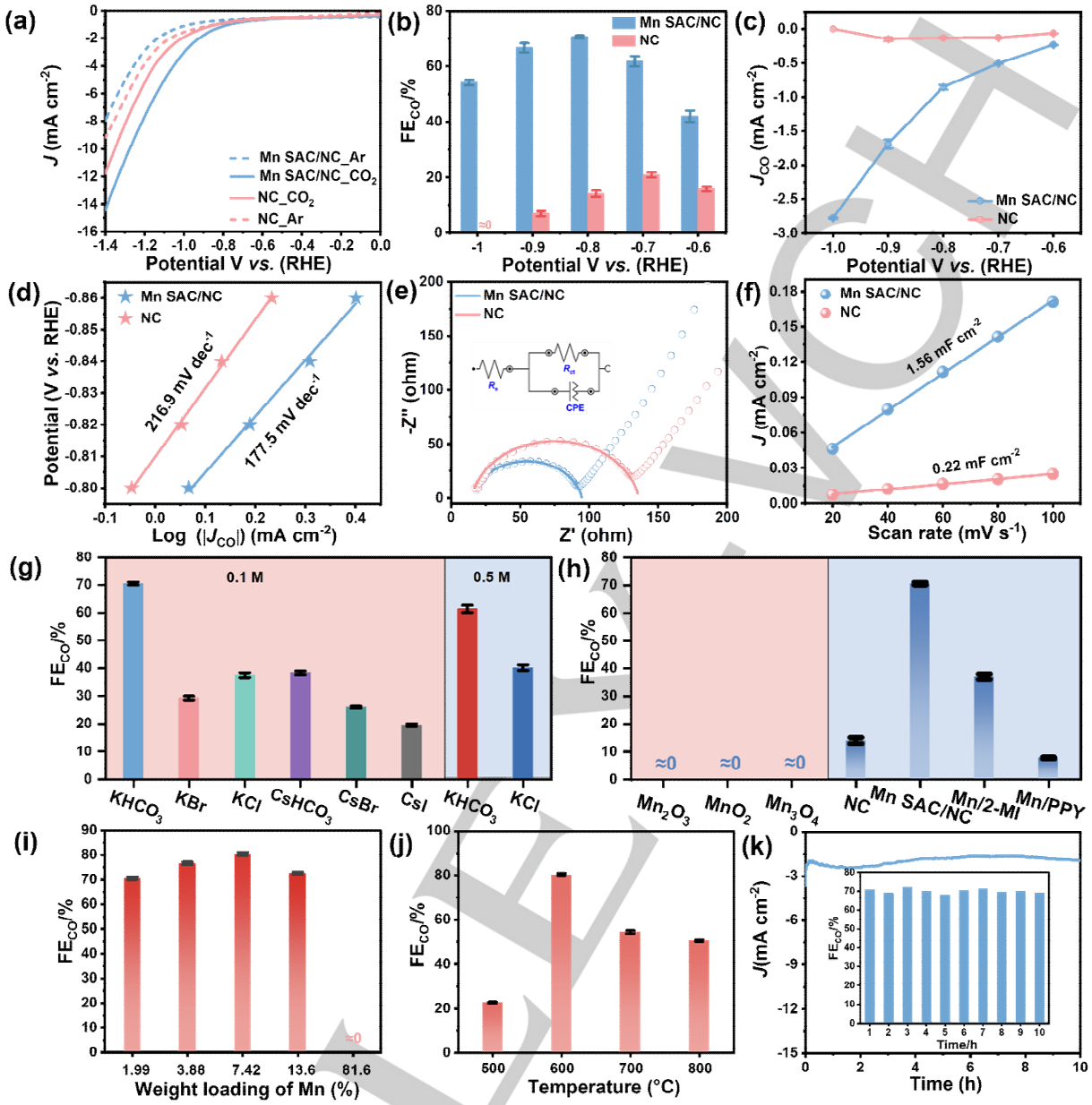

Figure 3. (a) LSV curves of Mn SAC/NC and NC in Ar (dashed line)- or CO_2 (solid line)-saturated 0.1 M $KHCO_3$ solution at a sweep rate of 5 mV s^{-1}. (b) FE_{CO} and (c) CO partial geometric current density over Mn SAC/NC and NC electrodes at different applied voltages. (d) Tafel plots and (e) Nyquist profiles of CO_2 electrolysis on Mn SAC/NC and NC. (f) C_{dl} of Mn SAC/NC and NC calculated from the current density of CV experiments as a function of scan rate. (g) FE_{CO} in various electrolytes at −0.8 V (vs. RHE). (h) FE_{CO} over various commercial Mn-based oxides, NC and Mn SAC/NC with different nitrogen-containing precursors at −0.8 V (*vs.* RHE). FE_{CO} as a function of different (i) Mn content and (j) calcinaion temperature at −0.8 V (*vs.* RHE). (k) ECR current density and FE_{CO} of Mn SAC/NC during 10 h of continuous electrolysis at −0.8 V (*vs.* RHE).

The electrocatalytic performance of Mn SAC/NC and NC for ECR was studied using a three-electrode system with 0.1 M $KHCO_3$ solution as electrolyte in an H-type cell. Figure 3a shows the linear sweep voltammetry (LSV) curves of Mn SAC/NC and NC. The current density in a CO_2-saturated electrolyte was obviously higher than that in an Ar-saturated electrolyte over the whole applied potential range, indicating the occurrence of ECR reaction. After the introduction of Mn single atoms, the current density under Ar atmosphere decreased compared to that with pure NC, which suggests that the HER was suppressed. Under CO_2-purged conditions, Mn SAC/NC exhibited larger cathodic

Based on the results from LSV tests, constant potential electrolysis was performed in a potential range from −0.6 V to −1 V with an interval of 0.1 V for 1 h (Figure 3b). The gas and liquid products were probed by gas chromatography (GC) and nuclear magnetic resonance (NMR) measurements, respectively (Figure S1). Only CO was detected as the ECR product together with H_2 generated from the competing HER. From the potential range of −0.6 V to −0.8 V, the FE_{CO} over Mn SAC/NC increased and achieved a maximum value of 70.7 ± 0.5 % at −0.8 V. Further elevating the overpotential, the FE toward CO dropped due to the enhanced HER (Figure S2). The FE_{CO} maintained over 50% at −1

V. As a contrast, the dominating product over NC was H_2 and the highest FE_{CO} only reached 21 ± 0.9 % at −0.7 V. Moreover, with the increase of the potential, only HER took place at −1 V. The results indicated that the incorporation of Mn single atoms into NC could substantially suppress the HER and boost the ECR selectivity for CO production. In addition, the CO partial geometric current density over Mn SAC/NC exceeds that of NC over the potential window, reaching −2.8 mA cm^{-2} at −1 V (Figure 3c).

To investigate the origin of the enhanced ECR performance over Mn SAC/NC, the interfacial reaction kinetics analysis for CO generation was performed through Tafel plots. As shown in Figure 3d, the Tafel slope of Mn SAC/NC is 177.5 mV dec^{-1}, much smaller than 216.9 mV dec^{-1} of NC. Thus, it can be inferred that Mn SAC/NC possessed a more favorable kinetics for the formation of $CO_2^{\bullet-}$ radical, which is the posssible rate-determining step for ECR reaction. Additionally, electrochemical impedance spectroscopy (EIS) study was carried out to reveal the charge transfer resistance of the electrocatalysts. Nyquist plots in Figure 3e indicated a faster surface charge transfer for Mn SAC/NC than that of NC during the ECR reaction, leading to the enhanced reaction activity. The electrochemical active surface area (ECSA) estimated from the double-layer capacitance (C_{dl}) was further calculated for Mn SAC/NC and NC (Figure 3f). The C_{dl} of Mn SAC/NC and NC was 1.56 and 0.22 mF cm^{-2}, respectively, which showed a similar C_{dl}, indicating that the Mn SAC/NC has a substantially larger ECSA than NC, facilitating the ECR process.

The dependance of ECR performance on different kinds of electrolytes was explored (Figure 3g). When using solution $CsHCO_3$ as the catholyte, a significant decrease in CO FE was observed, possibly because Cs^+ adsorbed on the surface of Mn SAC/NCblocked the active sites of ECR. When HCO_3^- was replaced with halide anions (e.g., Br, Cl, and I), a significant decrease in CO FE was observed. This may be due to the possibility that the halide anions occupied the active sites so that CO_2 cannot be efficiently adsorbed, resulting in drop of ECR performance.

The effect of nitrogen source on the electrocatalytic activity of Mn SAC/NC was studied using different nitrogen-containing ligands, including 2-methylimidazole (2-MI) and polypyrrole (PPY). The results showed that the 2,2'-bipyridine-5,5'-dicarboxylic acid precursor afforded the best ECR activity (Figure 3h). Hence it can be speculated that the precursor containing pyridine N is favorable for ECR on Mn SAC. For comparison, commercial Mn_2O_3, MnO_2, Mn_3O_4, and pure NC were also tested for ECR and were found to dominantly catalyze the HER, indicating the significant role of Mn single atoms and the interaction between Mn and the NC support. In addition, the ECR performance of Mn SAC/NC can be tuned through the regulation of Mn content. Increasing the Mn content from 1.99 wt% to 3.88 wt% and 7.42 wt%, the FE_{CO} was boosted from 70.7 ± 0.5 % to 76.9 ± 0.5 % and 80.5 ± 0.6 %, respectively. Whereas further increase of the Mn content to 13.6 wt % led to a drop of CO selectivity due to the enhanced HER (Figure 3i). When Mn NPs/NC (with a Mn content of 81.6%) was used for ECR, no CO_2 reduction products were detectable. This further highlights the critical importance of atomically dispersed Mn species for the ECR. Alternatively, the effect of thermal treatment temperature on the ECR performance was investigated (Figure 3j). The material calcined at 600 °C delivered the highest selectivity for CO in ECR reaction. Furthermore, a long-time stability test was conducted at −0.8 V in 0.1 M $KHCO_3$ solution, FE_{CO} and the ECR current density showed no decay on Mn SAC/NC within 10 h of consecutive electrolysis (Figure 3k), suggesting the excellent durability of Mn SAC/NC for the ECR reaction.

In order to study the durability of the catalyst during the ECR, post characterizations by XRD and HAADF-STEM were conducted for the catalyst after CO_2 electrolysis at −0.8 V for 1 h. No diffraction peaks from Mn clusters or nanoparticles or agglomerates were observed for Mn SAC/NC catalysts (Figure 4a). Single Mn atoms retained highly dispersal on the NC support (Figures 4b and S3), indicating good stability of the catalyst.

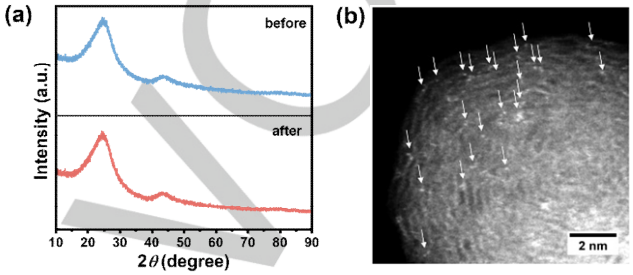

Figure 4. (a) XRD patterns of Mn SAC/NC before and after reaction. (b) High magnification HAADF-STEM image of Mn SAC/NC catalyst, with Mn single atoms indicated by white arrows, acquired after the reaction.

Conclusion

In summary, we have developed a facile method to synthesize Mn single atoms supported on N-doped carbon for the efficient ECR reaction to selectively produce CO. Compared with pure NC, the incorporation of Mn single atoms can effectively suppress the hydrogen evolution side reaction and boost the ECR activity. With an optimal Mn content of 7.42 wt%, the Mn SAC/NC obtained at 600 °C achieved an FE_{CO} of 80.5 ± 0.6 % at −0.8 V in 0.1 M $KHCO_3$ solution. Both the Mn single atom and its interaction with the NC from a suitable N-containing precursor were found to be critical to the ECR performance of the prepared material. The Mn SAC/NC exhibited good stability regarding almost unchanged FE_{CO} and ECR current density in the long-term electrolysis test. This work offers an alternative and flexible method for the preparation and regulation of Mn single atom catalysts toward valuable products from ECR reaction.

Experimental Section

Synthesis of Mn SAC/NC

1 g of pristine carbon black was dispersed in 150 mL of 5 M HNO_3 solution under bath ultrasonication, which was then subjected to heating at 90 °C for 4 h under refluxing. After repeatedly washing with water to ensure a pH value of approximately 7, the treated carbon black was finally vacuum-dried. 0.048 mmol of manganese acetate tetrahydrate and 0.096 mmol of 2,2'-bipyridine-5,5'-dicarboxylic acid were dispersed in 5 mL of ethanol and stirred for 1 h at room temperature. Then,120 mg of activated carbon black was added in the above solution and magnetically stirred for 4 h at 60 °C. Subsequently, the sample was dried at 60 °C overnight. Finally, the sample was annealed at 600 °C (or 500, 700, and 800 ºC) under N_2 atmosphere for 2 h with a ramping rate of 10 °C/min. Inductively coupled plasma-

atomic emission spectroscopy (ICP-AES) tests showed that the Mn weight content in the resulting Mn SAC/NC was 1.99%. Different Mn/NC samples with varying Mn weight contents (0, 3.88, 7.42, 13.6, and 81.6%) were fabricated by manipulating the amount of activated carbon black added using a similar experimental procedure. For the preparation of Mn/2-MI and Mn/PPY, 2,2'-2-methylimidazole and polypyrrole bipyridine-5,5'-dicarboxylic acid were used as the corresponding nitrogen precursors.

Electrochemical measurements

Typically, 1.2 mg of a catalyst was dispersed in 241.2 μL of a mixture containing isopropanol (IPA), deionized water, and 5 wt% Nafion solution with a corresponding volume ratio of 120: 120: 1.2 by bath ultrasonication for 30 min to form a homogeneous ink. The catalyst ink was then loaded onto a Toray carbon paper electrode with a size of 1.2 cm × 1 cm and dried under ambient conditions. For linear sweep voltammetry tests in Ar- or CO_2-saturated 0.1 M $KHCO_3$ solution, 1 mg of a catalyst was dispersed in the mixture of ethanol (100 μL), deionized water (100 μL), and Nafion solution (1 wt%, 100 μL). Then the mixture was ultrasonicated for 30 min to form a homogeneous ink. 7.95 μL of the ink was then loaded onto a glassy carbon electrode and dried under room temperature.

CO_2 electrolysis was tested in an H-type cell system with two compartments separated by a Nafion 117 membrane. Before ECR tests, the Nafion membrane was pre-treated by heating in 5% H_2O_2 aqueous solution and 0.5 M H_2SO_4 at 80 °C for 1 h, respectively. Subsequently, the Nafion membrane was immersed in deionized water under ambient conditions for 30 min and then washed with deionized water. Toray carbon fiber paper with a size of 1.2 cm × 1 cm was used as the working electrode. Pt wire and Ag/AgCl electrodes were used as the counter electrode and reference electrode, respectively. The potentials were controlled by an electrochemical working station (CHI 760E, Shanghai CH Instruments Co., China). All potentials stated in this work are relative to the reversible hydrogen electrode (RHE) scale unless otherwise mentioned. All potentials in this study (without compensation of voltage drop due to solution resistance, *iR*) were measured against the Ag/AgCl reference electrode (in saturated KCl solution) and converted to the RHE reference scale by

$$E\ (vs.\ \text{RHE}) = E\ (vs.\ \text{Ag/AgCl}) + 0.197 + 0.0591 \times \text{pH} \quad \text{(Eq. 1)}$$

ECR was conducted in CO_2-saturated 0.1 M $KHCO_3$ solution at room temperature and atmospheric pressure. The anolyte used in this work is 0.1 M H_2SO_4 solution unless stated otherwise. When saturated with CO_2, the pH of the catholyte was ~6.8. CO_2 with a flow rate of 10 mL·min^{-1} was purged into the $KHCO_3$ solution for at least 30 min to remove residual air in the reservoir, then controlled potential electrolysis was performed at each potential for 60 min.

Linear sweep voltammetry scans in Ar- or CO_2 atmosphere were carried out in a three-electrode system using Ag/AgCl as the reference electrode, Pt wire as the counter electrode, and glassy carbon as the working electrode with a CHI 760E potentiostat (CHI 760E, Shanghai CH Instruments Co., China). Rotating disk electrode (RDE) experiments were run on an AFMSRCE RDE control system (Pine Inc., USA). The catholyte used was 0.1 M $KHCO_3$ solution purged with Ar or CO_2 for at least 30 min. The anolyte used was 0.1 M H_2SO_4 solution.

Acknowledgements

This work was supported by the National Natural Science Foundation of China (No. 21972010, 22022503) and Beijing Natural Science Foundation (No. 2192039).

Conflict of Interest

The authors declare no conflict of interest.

Keywords: Electrocatalysis • Single-atom catalyst • CO • Mn • CO_2 reduction reaction

[1] T. Ma, Q. Fan, X. Lia, J. Qiu, T. Wu, Z. Sun, *J. CO_2 Util.* 2019, *30*, 168-182.
[2] X. Li, S. Hong, L. Hao, Z. Sun, *Chin. J. Chem. Eng.* **2022**, *43*, 143–151.
[3] W. Zhang, B. Jia, X. Liu, T. Ma, *SmartMat.* **2022**, *3*, 5–34.
[4] Q. Li, Y.-C. Wang, J. Zeng, X. Zhao, C. Chen, Q.-M. Wu, L.-M. Chen, Z.-Y. Chen, Y.-P. Le, *Rare Met.* **2021**, *40*, 3442–3453.
[5] B. Han, *Acta Phys. -Chim. Sin.* **2022**, *38*, 2012011.
[6] D.-C. Wang, L.-Yu, W. Jiao, Y.-F. Liu, C.-H. Mu, X. Jian, *Rare Met.* **2021**, *40*, 3–19.
[7] S. Guo, S. K. Zhao, X. Wu, H. Li, Y. Zhou, C. Zhu, N. Yang, X. Jiang, J. Ga o, L. Bai, Y. Liu, Y. Lifshitz, S.-T. Lee, Z. Kang, *Nat. Commun.* **2017**, *8*, 1828.
[8] J. H. Lee, S. Kattel, Z. Jiang, Z. Xie, S. Yao, B. M. Tackett, W. Xu, N. S. Mar inkovic, J. G. Chen, *Nat. Commun.* **2019**, *10*, 3724.
[9] D. M. Koshy, S. Chen, D. U. Lee, M. B. Stevens, A. M. Abdellah, S. M. Dull, G. Chen, D. Nordlund, A. Gallo, C. Hahn, D. C. Higgins, Z. Bao, T. F. Jaramillo, *Angew. Chem. Int. Ed.* **2020**, *59*, 4043–4050.
[10] F.-Y. Gao, S.-J. Hu, X.-L. Zhang, Y.-R. Zheng, H.-J. Wang, Z.-Z. Niu, P.-P. Yang, R.-C. Bao, T. Ma, Z. Dang, Y. Guan, X.-S. Zheng, X. Zheng, J.-F. Zhu, M.-R. Gao, S.-H. Yu, *Angew. Chem. Int. Ed.* **2020**, *59*, 8706–8712.
[11] H. Seong, V. Efremov, G. Park, H. Kim, J. S. Yoo, D. Lee, *Angew. Chem. I nt. Ed.* **2021**, *60*, 14563–14570.
[12] J. Wang, J. Yu, M. Sun, L. Liao, Q. Zhang, L. Zhai, X. Zhou, L. Li, G. Wan g, F. Meng, D. Shen, Z. Li, H. Bao, Y. Wang, J. Zhou, Y. Chen, W. Niu, B. Huan g, L. Gu, C.-S. Lee, and Z. Fan, *Small*, **2022**, *18*, 2106766.
[13] X. Deng, D. Alfonso, T.-D. Nguyen-Phan, D. R. Kauffman, *ACS Catal.* **2022**, *12*, 5921−5929.
[14] B. Qiao, A. Wang, X. Yang, L. F. Allard, Z. Jiang, Y. Cui, J. Liu, J. Li, T. Zha ng, *Nat. Chem.* **2011**, *3*, 634−641.
[15] M. Zhang, T.-S. Wu, S. Hong, Q. Fan, Y.-L. Soo, J. Masa, J. Qiu, Z. Sun, *A CS Sustainable Chem. Eng.* **2019**, *7*, 15030−15035.
[16] S. Chu, C. Kang, W. Park, Y. Han, S. Hong, L. Hao, H. Zhang, T. W. B. Lo, A. W. Robertson, Y. Jung, B. Han, Z. Sun, *SmartMat.* **2022**, *3*, 194–205.
[17] W. Li, L. Li, Q. Xia, S. Hong, L. Wang, Z. Yao, T.-S. Wu, Y.-L. Soo, H. Zhan g, T. W. B. Lo, A. W. Robertson, Q. Liu, L. Hao, Z. Sun, *Appl. Catal. B.* **2022**, *3 18*, 121823.
[18] Y. Jiang, Y. Sung, C. Choi, G.-J. Bang, S. Hong, X. Tan, T.-S. Wu, Y.-L. So o, P. Xiong, M. M.-J. Li, L. Hao, Y. Jung, Z. Sun, *Angew. Chem. Int. Ed.* **2022**, e 202203836.
[19] Y. Chen, L. Wang, Z. Yao, L. Hao, X. Tan, J. Masa, A.-W. Robertson, Z. Su n, *Acta Phys. -Chim. Sin.* **2022**, *38*, 2207024.
[20] Y. Huang, H. He, J. Liu, R. P. Thummel, L. Tong, *Chem. Asian. J.* 10.1002/ asia.202200217.
[21] Y. Gao, Y. Yang, L. Hao, S. Hong, X. Tan, T.-S. Wu, Y.-L. Soo, A. W. Rober tson, Q. Yang, Z. Sun, *Chem Catal.* **2022**, *2*, 1–14.
[22] V. Reddu, L. Sun, X. Li, H. Jin, S. Wang, X. Wang, *SmartMat.* **2022**, *3*, 151 –162.
[23] B. Chen, B. Li, Z. Tian, W. Liu, W. P. Liu, W. Sun, K. Wang, L. Chen, J. Jia ng, *Adv. Energy Mater.* **2021**, *11*, 2102152.
[24] X. Wang, Y. Wang, X. Sang, W. Zheng, S. Zhang, L. Shuai, B. Yang, Z. Li, J. Chen, L. Lei, N. M. Adli, M. K. H. Leung, M. Qiu, G. Wu, Y. Hou, *Angew. Che m. Int. Ed.* **2021**, *60*, 4192–4198.
[25] B. Chen, B. Li, Z. Tian, W. Liu, W.-P. Liu, W. Sun, K. Wang, L Chen, J. Jian g, *Adv. Energy Mater.* **2021**, *11*, 2102152.
[26] Y. Wu, C. Chen, X. Yan, X. Sun, Q. Zhu, P. Li, Y. Li, S. Liu, J. Ma, Y. Huan g, B. Han, *Angew. Chem. Int. Ed.* **2021**, *60*, 20803–20810.
[27] S. Wang, P. Zhou, L. Zhou, F. Lv, Y. Sun, Q. Zhang, L. Gu, H. Yang, S. Gu o, *Nano Lett.* **2021**, *21*, 4262−4269.
[28] H. Yang, L. Shang, Q. Zhang, R. Shi, G. I. N. Waterhouse, L. Gu, T. Zhang, *Nat. Commun.* **2019**, *10*, 4585.
[29] A. S. Varela, N. R. Sahraie, J. Steinberg, W. Ju, H.-S. Oh, P. Strasser, *Ang ew. Chem. Int. Ed* **2015**, *54*, 10758–10762.
[30] J. Feng, H. Gao, L. Zheng, Z. Chen, S. Zeng, C. Jiang, H. Dong, L. Liu, S. Zhang, X. Zhang, *Nat. Commun.* **2020**, *11*, 4341